Spectroscopy and laser operation of highly-doped 10 at.% Yb:$(Lu,Sc)_2O_3$ ceramics

Wei Jing[a], Pavel Loiko[b], Liza Basyrova[b], Yicheng Wang[c], Hui Huang[a], Patrice Camy[b], Uwe Griebner[c], Valentin Petrov[c], Josep Maria Serres[d], Rosa Maria Solé[d], Magdalena Aguiló[d], Francesc Díaz[d] and Xavier Mateos[d,e,*]

[a]*Institute of Chemical Materials, China Academy of Engineering Physics, 64 Mianshan Road, 621900 Mianyang, China*
[b]*Centre de recherche sur les Ions, les Matériaux et la Photonique (CIMAP), UMR 6252 CEA-CNRS-ENSICAEN, Université de Caen, 6 Boulevard du Maréchal Juin, 14050 Caen, France*
[c]*Max Born Institute for Nonlinear Optics and Short Pulse Spectroscopy, Max-Born-Str. 2a, 12489 Berlin, Germany*
[d]*Universitat Rovira i Virgili (URV), Física i Cristal·lografia de Materials i Nanomaterials (FiCMA-FiCNA)-EMaS, Marcel·lí Domingo 1, 43007 Tarragona, Spain*
[e]*Serra Húnter Fellow*
**Corresponding author, e-mail: xavier.mateos@urv.cat*

Abstract: Highly-doped "mixed" transparent sesquioxide ceramics, 10 at.% Yb:$(Lu_{2/3}Sc_{1/3})_2O_3$, are fabricated by vacuum sintering at 1700 °C followed by hot isostatic pressing (HIPing) at 1680 °C and 200 MPa. The ceramics are of single-phase nature with a cubic (C-type, a = 10.191 Å) structure and a mean grain size of 0.66 μm. They feature high low-signal transmission of 79.0% at 1.20 μm. The Yb^{3+} ions in "mixed" ceramics exhibit strong inhomogeneous broadening of the absorption and emission bands, with σ_{SE} of 0.43×10^{-20} cm^2 at 1079.4 nm and an emission bandwidth of 25.7 nm. The crystal-field splitting for Yb^{3+} ions is revealed at 12 K. The Yb ceramic laser generated a maximum peak output power of 250 mW at ~1.04 and 1.08 μm with a slope efficiency of 40.3%. The ceramics are promising for mode-locked lasers at ~1.08 μm, including thin-disk geometry.

Keywords: transparent ceramics; sesquioxides; ytterbium ion; luminescence; laser operation.

1. Introduction

Cubic rare-earth sesquioxides A_2O_3 (where A = Sc, Y or Lu) are well-known host crystals for doping with laser-active trivalent rare-earth ions such as ytterbium (Yb^{3+}) [1]. These materials exhibit attractive thermo-mechanical properties, such as high thermal conductivity (κ = 12.8 $Wm^{-1}K^{-1}$ for Lu_2O_3 with weak dependence on the Yb^{3+}-doping level [2]), isotropic thermal expansion and small and positive thermo-optic coefficients (dn/dT = 5.8×10^{-6} K^{-1} at 1 μm for Lu_2O_3) [3]. They are characterized by broadband transparency and relatively low maximum phonon energies for oxide crystals ($h\nu_{ph}$ = 614 cm^{-1} for Lu_2O_3) [4]. Yb^{3+} ions doped in cubic sesquioxides experience a strong crystal field leading to large total Stark splitting of the ground-state ($\Delta E(^2F_{7/2})$ = 903 cm^{-1} for Yb:Lu_2O_3) [5].

The interest in doping with Yb^{3+} ions is determined by their simple energy-level scheme potentially leading to high slope efficiencies and weak heat loading in such lasers. The spectroscopic features of Yb^{3+}-doped sesquioxide crystals enable broad tuning of the laser emission wavelength [6] and the generation of femtosecond laser pulses [7,8]. These materials were also found to be very suitable for thin-disk lasers and amplifiers [2,9].

The main drawback of A_2O_3 crystals is their high melting point (2450 °C for Lu_2O_3) which complicates the crystal growth. As a result, the most common approach for the growth of single crystals is the heat exchanger method (HEM) [10] using rhenium (Re) crucibles which may induce black coloration of the crystals due to Re impurities. An attractive alternative to the single-crystal growth is the technology of transparent polycrystalline ceramics. The latter can be fabricated at much lower temperatures while the attractive thermo-mechanical and spectroscopic properties of the material are in general well preserved [11,12]. Yb^{3+}-doped sesquioxide laser ceramics are now well-known [13,14].

An interesting feature of cubic sesquioxides is their ability to form solid-solutions $(A_xB_yC_z)_2O_3$ where $x + y + z = 1$ and A, B and C can stand for both passive (host-forming) and active (lasing) ions. The fabrication of such compositionally "mixed" materials is of interest because of the inhomogeneous broadening of the absorption and emission spectral bands of the active ions. The latter may lead to smoother and broader gain spectra which are attractive and beneficial for femtosecond mode-locked (ML) lasers. The growth and laser operation of Yb^{3+}-doped "mixed" sesquioxide single crystals were reported firstly by Schmidt *et al*. describing the growth of Yb:$(Lu,Sc)_2O_3$ crystals and their Kerr-lens mode-locked operation yielding 74 fs pulses at 1048 nm [15]. Thin-disk ML lasers based on "mixed" Yb:$(Lu,Sc)_2O_3$ and Yb:$(Lu,Sc,Y)_2O_3$ crystals have been demonstrated in [16,17]. The possibility to fabricate "mixed" sesquioxide materials was further exploited using the transparent ceramic technology [18,19]. Recently, Toci *et al*. reported on a diode-pumped CW Yb:$(Lu,Y)_2O_3$ ceramic laser delivering 2.7 W at 1078 nm with a slope efficiency of 48.1% [20].

In the present work, we focus on a "mixed" ceramics with high Yb^{3+}-doping, 10 at.% Yb:$(Lu,Sc)_2O_3$, for the first time, to the best of our knowledge. Highly-doped sesquioxide ceramics are also of interest for the thin-disk laser geometry [21]. Recently, we studied similar "mixed" $(Lu,Sc)_2O_3$ ceramics but doped with Tm^{3+} and Ho^{3+} ions [22,23] showing good potential for femtosecond pulse generation [24].

2. Fabrication of the laser ceramics

As starting materials, we used high-purity Yb_2O_3, Lu_2O_3 and Sc_2O_3 (5N) oxide powders. They were taken according to the formula $(Yb_{0.1}Lu_{0.6}Sc_{0.3})_2O_3$, i.e., assuming an Yb^{3+} doping level of 10 at.% (with respect to the host-forming cations, $Lu^{3+}|Sc^{3+}$) and well mixed. The mixture was ball milled in Teflon jars for 24 h at a speed of 200 rpm. After drying the slurry at 80 °C for 24 h, the powder was sifted with a 200-mesh screen and calcinated at 400 °C for 4 h. The green ceramic sample was dry-pressed into a disk by applying a uniaxial pressure of 20 MPa, and further cold isostatically pressed at 200 MPa to increase its density. Prior to the densification sintering, the sample was calcined at a temperature 1000 °C for 10 h. This helped to remove unwanted organic impurities and residual carbon. Then, the Yb:$(Lu,Sc)_2O_3$ disk was subjected to vacuum sintering at 1700 °C followed by hot isostatic pressing (HIPing) at 1680 °C and 200 MPa in argon atmosphere for 2 h. The obtained ceramic was annealed at 1500 °C for 8 h in air to remove oxygen vacancies. The ceramic disks were polished to laser-grade quality from both sides.

A photograph of polished ceramic disks is shown in Fig. 1. They are transparent and colorless.

3. Experimental

The morphology of a thermally etched surface of the ceramic disk was studied by Field Emission Scanning Electron Microscopy (FESEM) using a JEOL JSM-6700 microscope. The grain size distribution was determined using the ImageJ software. The phase composition of the ceramic was identified by X-ray powder diffraction (XRD) employing a Tongda DX–1000CSC diffractometer and Cu Kα radiation (1.54056 Å). The XRD patterns were measured for the 2θ range of 10° - 80° with a scan speed of 1.2°/min and a step size of 0.02°.

The room temperature (RT, 293 K) Raman spectra were measured using a confocal microscope (inVia, Renishaw) equipped with a ×50 objective (Leica) and an Ar^+ ion laser (488.0 nm).

The RT absorption and transmission spectra were measured using a spectrophotometer (Lambda 1050, Perkin Elmer). The luminescence spectrum was measured using an optical spectrum analyzer (OSA, Ando AQ6315-E) employing a Ti:Sapphire laser tuned to 920 nm as an excitation source. The luminescence decay was studied employing a ns optical parametric oscillator (OPO, Horizon, Continuum), a 1/4 m monochomator (Oriel 77200), an InGaAs detector and an 8 GHz digital oscilloscope (DSA70804B, Tektronix).

For low-temperature (LT, 12 K) studies, the sample was mounted on an APD DE-202 closed-cycle cryo-cooler equipped with an APD HC 2 Helium vacuum cryo-compressor and a Laceshore 330 temperature controller. The LT absorption spectrum was measured using a 20 W halogen lamp with a spectrally calibrated emission and the OSA. The LT luminescence spectrum was measured using the same OSA. The spectral resolution was 0.2 nm.

4. Characterization of the ceramics

4.1. Structural study

A typical FESEM image of the polished and thermally etched surface of the ceramic is shown in Fig. 2. The ceramic features a close-packed microstructure without pores and secondary phases at the grain boundaries. The grain size distribution is shown in the inset of Fig. 2. The grain size was determined by the linear intercept method using a shape factor of 1.2; a total of 150 grains were counted for an area of ~10×10 μm^2. The distribution is relatively narrow and the mean grain size D_{grain} is 0.66 μm.

The powder XRD pattern of the ceramics is shown in Fig. 3. The Yb:$(Lu,Sc)_2O_3$ ceramic is of single-phase nature. It is cubic (sp. gr. $Ia\bar{3}$ - T^7_h, No. 206) and possesses the so-called bixbyite ($(Mn,Fe)_2O_3$-type) or C-type structure [25], the same as the parent Lu_2O_3 and Sc_2O_3 compounds. The lattice constant was determined with the profile matching method using the FULLPROF software, a = 10.191 Å. It occupies an intermediate position between those for Lu_2O_3 (a = 10.391 Å) and Sc_2O_3 (a = 9.857 Å) [1]. Note that the stoichiometric cubic phase Yb_2O_3 also exists. In the bixbyite structure, there are two crystallographic sites for Yb^{3+} ions replacing for the host-forming cations Lu^{3+} and Sc^{3+}. The site symmetries are C_2 and C_{3i} and both are VI-fold oxygen coordinated. The ratio of the C_2 to C_{3i} sites is 3:1, i.e., there are 32 cations in a unit cell in which 24 occupy the C_2 sites and 8 occupy the C_{3i} ones. The optical properties of cubic sesquioxides are mainly determined by most ions (approximately 3/4) residing in the C_2 sites (for the C_{3i} ones, the electric-dipole (ED) transitions are forbidden due to the inversion symmetry). The compositional disorder and the difference in the ionic radii of Yb^{3+} (0.868 Å), Lu^{3+} (0.861 Å) and especially Sc^{3+} (0.745 Å) [26] is expected to promote the inhomogeneous broadening of the Yb^{3+} spectral bands.

The Raman spectrum of the Yb:$(Lu,Sc)_2O_3$ ceramic is shown in Fig. 4. The factor group analysis predicts the following irreducible representations at the Γ-point ($\boldsymbol{k}$ = 0): $\Gamma = 4A_g + 4E_g + 14F_g + 5A_u + 5E_u + 17F_u$ of which 22 even (*gerade*) modes (A_g, E_g and F_g) are Raman-active, 17 modes (F_u) are IR-active and the rest are silent [27]. The measured Raman spectrum is typical for cubic sesquioxides [4] but it is significantly broadened as compared, e.g., to that for the Yb:Lu_2O_3 ceramics. The most intense band is observed at 388 cm^{-1} (its full width at half maximum, FWHM, is 45 cm^{-1}) and it is assigned to $A_g + F_g$ vibrations. The maximum phonon energy $h\nu_{ph}$ is 689 cm^{-1}.

4.2. Optical spectroscopy

The small-signal transmission spectrum of the ceramics in the range of 250-1200 nm (recalculated for the reference thickness of 1.0 mm) is shown in Fig. 5. It contains a strong structured absorption band at ~1 μm due to the $^2F_{7/2} \rightarrow {}^2F_{5/2}$ Yb^{3+} transition and a broad band at ~0.3 μm overlapping with the absorption edge which is assigned to residual pores. The optical bandgap was determined from the Tauc plot assuming direct transitions [28], i.e., by plotting $(\alpha_{abs} \times h\nu)^2$ *vs*. the photon energy $h\nu$, where α_{abs} is the absorption coefficient, as shown as inset of Fig. 5. Note that undoped Lu_2O_3 has a direct band gap and it remains so under rare-earth doping [29]. For the studied ceramic, E_g is 4.64 eV (λ_g = 267 nm).

The small-signal transmission T_0 at ~1.2 μm (out of Yb^{3+} absorption) is 79.0% and it is close to the theoretical value T_{Fr} = 81.0% determined by the Fresnel losses assuming a refractive index $\langle n \rangle$ of 1.925 for the composition of $(Lu_{2/3}Sc_{1/3})_2O_3$ [30]. This result is much

better than for the translucent Yb:$(Lu,Sc)_2O_3$ ceramics reported in [18] having a transmission of only 46.2% at ~1.2 μm, highlighting the good optical quality.

The absorption cross-sections were calculated as $\sigma_{abs} = \alpha_{abs}/N_{Yb}$, where $N_{Yb} = 28.5\times10^{20}$ cm^{-3} is the Yb^{3+} ion density. Sometimes for rare-earth-doped sesquioxides, the absorption cross-sections are calculated by considering only the ions residing in C_2 sites, i.e., by taking about 3/4 of the total doping concentration. However, in the case of a "mixed" material, the distribution of Lu^{3+} and Sc^{3+} cations over the C_2 and C_{3i} sites is unknown. One may expect that Yb^{3+} ions will mostly replace the Lu^{3+} ones (due to the closeness of their ionic radii), so that the "ideal" distribution over the two sites will be disturbed. In this way, we consider the σ_{abs} values as "effective" ones.

The RT σ_{abs} spectrum of the Yb:$(Lu,Sc)_2O_3$ ceramic is given in Fig. 6(a) and compared with Yb:Lu_2O_3 and Yb:Sc_2O_3 single-crystals [31]. For the "mixed" ceramic, the maximum σ_{abs} is 1.82×10^{-20} cm^2 at 976.0 nm and the FWHM of the absorption peak is 5.5 nm. This peak corresponds to the so-called zero-phonon-line (ZPL) in absorption for the Yb^{3+} ion, i.e., the transition between the lowest Stark sub-levels of the multiplets, 0 → 0'. It is split at RT showing two components at 973.5 nm and 976.0 nm. The ZPL for the "mixed" ceramics is notably broadened and reduced in intensity as compared to those for the single-crystalline sesquioxides. This is related to (i) the polycrystalline nature of the ceramic and (ii) the compositional disorder in the "mixed" material. Indeed, for Yb:Lu_2O_3 crystal, the maximum σ_{abs} is 3.06×10^{-20} cm^2 at 975.4 nm with a FWHM of 2.9 nm [31]. Strong spectral broadening is also observed for the entire absorption spectrum of the "mixed" ceramic, representing the effect of inhomogeneous spectral broadening.

The stimulated-emission (SE) cross-section, σ_{SE}, was calculated by two methods. The first one is the Füchtbauer–Ladenburg (F-L) equation [32]:

$$\sigma_{SE}(\lambda) = \frac{\lambda^5}{8\pi < n >^2 \tau_{rad} c} \frac{W'(\lambda)}{\int \lambda W'(\lambda) d\lambda}, \quad (1)$$

where, λ is the light wavelength, $<n>$ is the refractive index of the host matrix corresponding to the average luminescence wavelength $<\lambda_{lum}>$, τ_{rad} is the radiative lifetime of the upper manifold ($^2F_{5/2}$ for Yb^{3+} ions), c is the speed of light and $W'(\lambda)$ is the luminescence spectrum accounting for the apparatus function of the set-up determined using a spectrally-calibrated light source.

The second one is the reciprocity method (RM), or McCumber equation [33]:

$$\sigma_{SE}(\lambda) = \sigma_{abs}(\lambda) \frac{Z_1}{Z_2} \exp\left(-\frac{hc/\lambda - E_{ZPL}}{kT}\right), \quad (2)$$

where h is the Planck constant and (hc/λ) is the photon energy, k is the Boltzmann constant, T is the considered temperature (RT), E_{ZPL} is energy corresponding to the ZPL transition, and Z_m are the so-called partition functions of the lower (m = 1, $^2F_{7/2}$) and upper (m = 2, $^2F_{5/2}$) manifolds of the Yb^{3+} ion:

$$Z_m = \sum_k g_k^m \exp(-E_k^m / kT). \quad (3)$$

In Eq. (3), $g^m_k = 1$ is the degeneracy of the Stark sub-level with the number k and energy E^m_k which is measured from the lowest sub-level of each multiplet.

The SE cross-sections calculated by the two different methods show good agreement for a τ_{rad} value of 0.79±0.01 ms. It agrees well with the lifetimes reported for Yb:Lu_2O_3 (0.82 ms) and Yb:Sc_2O_3 (0.80 ms) [31].

The SE cross-section spectrum of the Yb:$(Lu,Sc)_2O_3$ ceramic obtained by combining the data from the F-L equation and the RM (to avoid the effect of reabsorption on the measured luminescence spectra) is shown in Fig. 6(b). The maximum σ_{SE} is 1.95×10^{-20} cm^2 at 976.0 nm corresponding to the ZPL. At longer wavelengths where laser operation is expected, σ_{SE} is 0.89×10^{-20} cm^2 at 1034.0 nm (FWHM = 19.2 nm) and 0.43×10^{-20} cm^2 at 1079.4 nm (FWHM = 25.7 nm). Similar to the absorption spectrum, the emission band indicates strong inhomogeneous broadening as compared to the parent sesquioxides. Indeed, for Yb:Lu_2O_3, σ_{SE} is 0.44×10^{-20} cm^2 at 1079.1 nm with a FWHM of only 15.4 nm [31].

The Yb^{3+} ion represents a quasi-three-level laser scheme with reabsorption. Thus, it is useful to calculate the gain cross-section, $\sigma_g = \beta\sigma_{SE} - (1 - \beta)\sigma_{abs}$, where $\beta = N_2(^2F_{5/2})/N_{Yb}$ is the inversion ratio and N_2 is the fraction of active ions in the upper laser level, to conclude about the expected laser wavelength. The gain spectra for the Yb:$(Lu,Sc)_2O_3$ ceramic are shown in Fig. 7. For small inversion ratios $\beta < 0.08$, there is a local peak centered at ~1079 nm. For higher β, another peak at ~1034 nm appears.

The luminescence decay curve was measured at RT for a finely powdered ceramic sample (to avoid the effect of reabsorption on the measured lifetime), see Fig. 8. It is well fitted with a single-exponential law yielding a luminescence lifetime of τ_{lum} = 159 μs. For comparison, in Fig. 8, we also provide the decay curve for a bulk ceramic corresponding to longer τ_{lum} of 172 μs due to the reabsorption. The uncertainty of the determined lifetimes is ±5 μs. The determined τ_{lum} value is much shorter than the radiative one corresponding to a luminescence quantum yield of $\eta_q = \tau_{lum}/\tau_{rad} \approx 20\%$. The latter is an indication of strong concentration-quenching of luminescence. It is assigned to energy migration to defects and impurities. For example, we cannot exclude the presence of Zr^{4+} ions in the fabricated ceramics (zirconia was used in the grinding balls and milling jar). The luminescence decay curve can be then represented as $I(t) = I_0\times\exp(-(t/\tau_0) - \omega t)$, where $I(t)$ is the luminescence intensity, t is time, τ_0 is the intrinsic lifetime in the limit of low doping level and ω is the energy-migration rate expressed in s^{-1}. In the case of Yb^{3+} showing no energy-transfer upconversion, the decay curve under strong energy-migration is expected to maintain the single-exponential shape.

To reveal the crystal-field splitting of the Yb^{3+} ion, the LT absorption and luminescence spectra were measured as shown in Fig. 9. For Yb^{3+} ions in the C_2 sites, each $^{2S+1}L_J$ multiplet is split into J+1/2 sub-levels which are numbered as 0 .. 3 and 0' .. 2' (in the order of increasing energy) for the lower and upper manifolds of Yb^{3+}, respectively. The assignment of the LT spectra is according to Ref. [5]. The spectra of the "mixed" ceramic remain broad even at low temperatures when the electron-phonon interaction is nearly suppressed. Indeed, for the emission peak associated with the 0' → 3 electronic transition, the emission bandwidth (FWHM) is 18.6 nm. The composite nature of the ZPL is preserved at LT with two

components at 971.8 and 975.6 nm. In the previous work on Yb^{3+}-doped sesquioxides [34], the splitting of the ZPL in absorption was also described at LT (10 K): for Yb:Lu_2O_3, two peaks at 974.4 and 975.6 nm were observed leading to different emission spectra assigned to Yb^{3+} ions in C_{3i} and C_2 sites, respectively. In our case, a selective excitation of the "mixed" ceramic into two spectral components of the ZPL did not lead to any noticeable difference in the LT luminescence spectra, cf. Fig. 9, both assigned to Yb^{3+} ions in C_2 sites. Moreover, the relative intensity of the spectral components of the ZPL for the studied ceramic disagree with that for the Yb:Lu_2O_3 crystal [34]. Thus, we suggest the following explanation: as a consequence of the structural disorder, the second coordination sphere around Yb^{3+} can be constituted by various combinations of the Sc^{3+}, Lu^{3+} and Yb^{3+} ions, some of them different at the point to generate crystal fields around a given site (C_2) sufficiently different to give rise to distinct ZPLs.

The Yb^{3+} energy-level scheme in "mixed" $(Lu,Sc)_2O_3$ ceramic is shown in Fig. 10. The corresponding set of energy-levels is $^2F_{7/2}$ = (0, 459, 562, 985) cm^{-1} and $^2F_{5/2}$ = (10250, 10703, 11067) cm^{-1}. For comparison, we also provide the data for Lu_2O_3 and Sc_2O_3 [31]. For most of the Stark components, their energies are intermediate between those for the parent compounds. The total Stark splitting of the ground-state $\Delta E(^2F_{7/2})$ is 985 cm^{-1}. The partition functions Z_1 = 1.175 and Z_2 = 1.126 and their ratio Z_1/Z_2 = 1.044 (at RT).

Note that there exists a slightly different assignment of the low-temperature spectra for Yb^{3+} in C_2 sites in Lu_2O_3 [35]. The main difference from our work is the position of the sub-levels 1 ($^2F_{7/2}$) and 1' ($^2F_{5/2}$). The corresponding peaks in the LT spectra are marked by the asterisks.

5. Laser operation

5.1. Laser set-up

The scheme of the laser set-up is shown in Fig. 11. The Yb:$(Lu,Sc)_2O_3$ ceramic sample with a thickness of 2.61 mm and an aperture of 3.0×3.0 mm^2 was mounted on a passively cooled Cu-holder using a silver paint for better thermal contact. The nearly hemispherical cavity was formed by a flat pump mirror (PM) coated for high transmission (HT, $T > 97\%$) at 0.88-0.99 μm and for high reflection (HR, $R > 99.9\%$) at 1.02-1.20 μm, and a set of concave output couplers (OCs) having a radius of curvature (RoC) of -100 mm and a transmission in the range of 1% - 10% (±0.5%) at 1.0-1.1 μm. The cavity length was about ~100 mm. The laser element was placed close to the PM with an airgap less than ~1 mm.

As a pump source, we used a CW Ti:Sapphire laser (3900S, Spectra Physics) emitting in the fundamental mode (TEM_{00}, $M^2 \approx 1$) and delivering up to ~2.3 W at 966.4 nm. The pump power was varied by a rotatable half-wave plate and a Glan-Taylor polarizer. The pump was focused into the laser element through the PM using an achromatic antireflection (AR) coated lens (f = 50 mm) resulting in a pump spot size at the focus $2w_P$ of 60±5 μm. The diameter of the laser mode in the ceramic element was calculated with the ABCD method as $2w_L$ = 55±10 μm. As all the OCs provided high reflectance at the pump wavelength ($R >$ 90%), pumping was in double-pass. The pump absorption under lasing conditions, $\eta_{abs,L(2\text{-pass})} = P_{abs}/P_{inc}$, was determined from pump-transmission measurement at the threshold pump

power accounting for the double-pass of the pump. It slightly decreased with output coupling, from 85.5% (T_{OC} = 1%) to 85.0% (T_{OC} = 10%). Note that these values include the Fresnel losses at the uncoated ceramic element. The residual pump was blocked by a cut-on filter (FEL1000, Thorlabs). The laser spectra were measured using an optical spectrum analyzer (OSA, Ando AQ6315-E).

5.2. Laser performance

First, the laser performance was studied for a pump wavelength λ_P of 966.4 nm (its choice will be argued below). The input-output dependences for a duty-cyle of 1:2 are shown in Fig. 12(a). The Yb:$(Lu,Sc)_2O_3$ ceramic laser generated a maximum peak output power of 250 mW at 1038-1042 and 1075-1088 nm with a slope efficiency η of 40.3% (*vs*. the absorbed pump power P_{abs}) and a laser threshold P_{th} of 0.82 W (for T_{OC} = 10%). The output dependence was nonlinear near the threshold, so that its fitting was performed for pump powers well exceeding P_{th}. The optical-to-optical efficiency *vs*. the pump power incident on the crystal η_{opt} was 11.8%. Further power scaling was limited by the available pump, P_{inc} ~2.1 W. For lower output coupling, the laser threshold gradually decreased reaching 0.47 W for T_{OC} = 1%. The relatively high values of the laser thresholds are due to the relatively short luminescence lifetime (Fig. 8) in the highly doped ceramic. The simulation of the laser threshold for a quasi-three-level laser [36] yields a round-trip passive loss L of ~13%.

The typical spectra of the laser emission are shown in Fig. 12(b). For low output coupling (1% – 5%), the emission was centered at ~1.08 μm. The spectra experienced a slight blue-shift with T_{OC}, namely from 1081-1084 nm (T_{OC} = 1%) to 1077-1081 nm (T_{OC} = 5%). For higher T_{OC} = 10%, the emission occurred within two ranges centered at ~1.04 and 1.08 μm. This behavior is due to the quasi-three-level nature of the Yb^{3+} laser scheme exhibiting weaker reabsorption for higher output coupling and it is in line with the gain spectra, Fig. 7.

We have also studied the effect of the pump duty cycle on the laser performance for the same T_{OC} = 10%, Fig. 12(c). Using a duty cycle of 1:6, the maximum peak output power slightly improved to 284 mW corresponding to η = 40.7%. For true CW operation, a thermal roll-over was observed for P_{abs} > 1.7 W resulting in a maximum output power of only 173 mW. This indicates thermal effects in the ceramic laser element which was only passively cooled.

The laser excitation spectrum for the Yb:$(Lu,Sc)_2O_3$ ceramic laser (the dependence of the peak output power on the pump wavelength) is shown in Fig. 13. The incident pump power was almost constant across this range of λ_P, P_{inc} ~ 2.1 W. For comparison, we also show the small-signal single-pass pump absorption in the laser element, $\eta_{abs,0} = 1 - \exp(-\sigma^P_{abs} N_{Yb} t)$. Laser action was achieved when tuning the pump wavelength between 888.8 and 990.7 nm. Interestingly, the laser excitation spectrum followed the $\eta_{abs,0}$ dependence except for the ranges where the pump was almost completely absorbed. The latter is especially clear in the vicinity of the zero-phonon-line of Yb^{3+}. This behavior can be explained by significant reabsorption losses in unpumped areas of the highly doped laser element. As a result, selecting the pump wavelength out of the main absorption peaks resulted in a more uniform distribution of absorbed pump power along the laser element and more uniform inversion.

Two pump wavelengths λ_P were thus selected, 966.4 nm and 932.0 nm. The difference between them is related the heat load. The fractional heat load, η_h, is estimated from the Stokes efficiency as $\eta_h \approx \eta_{St,L} = 1 - \lambda_P/\langle\lambda_L\rangle$ yielding 10.3% and 13.5%, respectively (assuming a mean laser wavelength $\langle\lambda_L\rangle$ of 1078 nm). Thus, more pronounced thermal effects are expected when pumping at λ_P = 932.0 nm. The corresponding input-output dependence is shown in Fig. 12(a). The quasi-CW laser generated a maximum output power of 304 mW (due to the slightly higher available pump) whilst with a reduced η of 33.5% and increased P_{th} of 0.88 W.

6. Conclusions

To conclude, we report for the first time on the synthesis, spectroscopic characterization and laser operation of compositionally "mixed" sesquioxide ceramics $(Lu_{2/3}Sc_{1/3})_2O_3$ highly doped with Yb^{3+} ions. These materials exhibit a relatively narrow grain size distribution and sub-μm grain size, high optical transparency and significant inhomogeneous broadening of the spectral bands. At the wavelength where the laser operation is expected (~1079 nm), the stimulated-emission cross-section is 0.43×10^{-20} cm^2 corresponding to an emission bandwidth (FWHM) of 25.7 nm. The estimated radiative lifetime of Yb^{3+} is 0.79 ms. The crystal-field splitting for Yb^{3+} ions in C_2 sites is revealed at low temperature (12 K). CW laser operation is achieved in the fabricated ceramics yielding an output power of 173 mW with a slope efficiency of 24.6%. Reducing the thermal load in the ceramics by operating in quasi-CW at a duty-cycle of 1:2 a maximum peak output power of 250 mW at ~1.04 and 1.08 μm with a slope efficiency of 40.3% was measured. The laser performance is strongly affected by the reabsorption losses. The fabricated ceramics are of interest for mode-locked oscillators. Further optimization of the synthesis procedure is needed to reveal the nature of the strong concentration quenching of luminescence (e.g., by eliminating uncontrolled rare-earth impurities via purification of the raw materials).

Acknowledgements

This work was supported by Spanish Government, Ministry of Science and Innovation (project No. PID2019-108543RB-I00) and by Generalitat de Catalunya (project No. 2017SGR755). Wei Jing acknowledges financial support from the National Natural Science Foundation of China (grant No. 61805219) and the Key Laboratory of Science and Technology on High Energy Laser, CAEP.

References

1. C. Kränkel, Rare-earth-doped sesquioxides for diode-pumped high-power lasers in the 1-, 2-, and 3-μm spectral range, IEEE J. Sel. Top. Quantum Electron. 21 (2014) 250-262.
2. R. Peters, C. Kränkel, S.T. Fredrich-Thornton, K. Beil, K. Petermann, G. Huber, O.H. Heckl, C.R.E. Baer, C.J. Saraceno, T. Südmeyer, U. Keller, Thermal analysis and efficient high power continuous-wave and mode-locked thin disk laser operation of Yb-doped sesquioxides, Appl. Phys. B 102 (2011) 509-514.

3. P.A. Loiko, K.V. Yumashev, R. Schödel, M. Peltz, C. Liebald, X. Mateos, B. Deppe, C. Kränkel, Thermo-optic properties of Yb:Lu_2O_3 single crystals, Appl. Phys. B 120 (2015) 601–607.
4. L. Laversenne, Y. Guyot, C. Goutaudier, M.T. Cohen-Adad, G. Boulon, Optimization of spectroscopic properties of Yb^{3+}-doped refractory sesquioxides: cubic Y_2O_3, Lu_2O_3 and monoclinic Gd_2O_3, Opt. Mater. 16 (2001) 475-483.
5. V. Peters, Growth and spectroscopy of ytterbium-doped sesquioxides, Dissertation (Shaker Verlag, Aachen, Germany, 2001).
6. R. Peters, C. Kränkel, K. Petermann, G. Huber, Broadly tunable high-power Yb:Lu_2O_3 thin disk laser with 80% slope efficiency, Opt. Express 15 (2007) 7075-7082.
7. U. Griebner, V. Petrov, K. Petermann, V. Peters, Passively mode-locked Yb:Lu_2O_3 laser, Opt. Express 12 (2004) 3125-3130.
8. P. Klopp, V. Petrov, U. Griebner, K. Petermann, V. Peters, G. Erbert, Highly efficient mode-locked Yb:Sc_2O_3 laser, Opt. Lett. 29 (2004) 391-393.
9. S. V. Marchese, C. R. E. Baer, R. Peters, C. Kränkel, A. G. Engqvist, M. Golling, D. J. H. C. Maas, K. Petermann, T. Südmeyer, G. Huber, U. Keller, Efficient femtosecond high power Yb:Lu_2O_3 thin disk laser, Opt. Express 15 (2007) 16966-16971.
10. R. Peters, C. Kränkel, K. Petermann, G. Huber, Crystal growth by the heat exchanger method, spectroscopic characterization and laser operation of high-purity Yb:Lu_2O_3, J. Cryst. Growth 310 (2008) 1934-1938.
11. J. Lu, K. Takaichi, T. Uematsu, A. Shirakawa, M. Musha, K.I. Ueda, H. Yagi, T. Yanagitani, A.A. Kaminskii, Yb^{3+}:Y_2O_3 ceramics–a novel solid-state laser material, Jpn. J. Appl. Phys. 41 (2002) L1373-L1375.
12. Z. Liu, G. Toci, A. Pirri, B. Patrizi, J. Li, Z. Hu, J. Wei, H. Pan, T. Xie, M. Vannini, J. Li, Fabrication and laser operation of Yb:Lu_2O_3 transparent ceramics from co-precipitated nano-powders, J. Am. Ceram. Soc. 102 (2019) 7491-7499.
13. J. Kong, D.Y. Tang, B. Zhao, J. Lu, K. Ueda, H. Yagi, T. Yanagitani, 9.2-W diode–end–pumped Yb:Y_2O_3 ceramic laser, Appl. Phys. Lett. 86 (2005) 161116.
14. J. Lu, J. F. Bisson, K. Takaichi, T. Uematsu, A. Shirakawa, M. Musha, K. Ueda, H. Yagi, T. Yanagitani, A. A. Kaminskii, Yb^{3+}:Sc_2O_3 ceramic laser, Appl. Phys. Lett. 83 (2003) 1101-1103.
15. A. Schmidt, V. Petrov, U. Griebner, R. Peters, K. Petermann, G. Huber, C. Fiebig, K. Paschke, G. Erbert, Diode-pumped mode-locked Yb:$LuScO_3$ single crystal laser with 74 fs pulse duration, Opt. Lett. 35 (2010) 511-513.
16. C. R. E. Baer, C. Kränkel, O. H. Heckl, M. Golling, T. Südmeyer, R. Peters, K. Petermann, G. Huber, U. Keller, 227-fs pulses from a mode-locked Yb:$LuScO_3$ thin disk laser, Opt. Express 17 (2009) 10725-10730.
17. K. Beil, C.J. Saraceno, C. Schriber, F. Emaury, O.H. Heckl, C.R. Baer, M. Golling, T. Südmeyer, U. Keller, C. Kränkel, G. Huber, Yb-doped mixed sesquioxides for ultrashort pulse generation in the thin disk laser setup, Appl. Phys. B 113 (2013) 13-18.
18. W. Liu, H. Kou, J. Li, B. Jiang, Y. Pan, Transparent Yb:$(Lu_xSc_{1-x})_2O_3$ ceramics sintered from carbonate co-precipitated powders, Ceram. Intern. 41 (2015) 6335-6339.
19. S. Lu, Q. Yang, H. Zhang, Y. Wang, D. Huang, Fabrication and spectral properties of Yb:$(Sc_{0.9}Y_{0.1})O_3$ transparent ceramics, Opt. Mater. 35 (2013) 793-797.

20. G. Toci, A. Pirri, B. Patrizi, R.N. Maksimov, V.V., Osipov, V.A. Shitov, M. Vannini, Yb^{3+}:$(Lu_xY_{1-x})_2O_3$ mixed sesquioxide ceramics for laser applications. Part II: Laser performances, J. Alloy Compd. 853 (2020) 156943.
21. H. Nakao, T. Inagaki, A. Shirakawa, K. Ueda, H. Yagi, T. Yanagitani, A. A. Kaminskii, B. Weichelt, K. Wentsch, M. A. Ahmed, T. Graf, Yb^{3+}-doped ceramic thin-disk lasers of Lu-based oxides, Opt. Mater. Express 4 (2014) 2116-2121.
22. W. Jing, P. Loiko, J.M. Serres, Y. Wang, E. Vilejshikova, M. Aguiló, F. Díaz, U. Griebner, H. Huang, V. Petrov, X. Mateos, Synthesis, spectroscopy and efficient laser operation of "mixed" sesquioxide Tm:$(Lu,Sc)_2O_3$ transparent ceramics, Opt. Mater. Express 7 (2017) 4192-4202.
23. W. Jing, P. Loiko, J.M. Serres, Y. Wang, E. Vilejshikova, X. Mateos, M. Aguiló, F. Díaz, U. Griebner, H. Huang, V. Petrov, Synthesis, spectroscopy and laser operation of "mixed" Ho:$(Lu,Sc)_2O_3$ ceramics, J. Lumin. 203 (2018) 145-151.
24. Y. Wang, W. Jing, P. Loiko, Y. Zhao, H. Huang, X. Mateos, S. Suomalainen, A. Härkönen, M. Guina, U. Griebner, V. Petrov, Sub-10 optical-cycle passively mode-locked Tm:$(Lu_{2/3}Sc_{1/3})_2O_3$ ceramic laser at 2 μm, Opt. Express 26 (2018) 10299-10304.
25. M. Guzik, J. Pejchal, A. Yoshikawa, A. Ito, T. Goto, M. Siczek, T. Lis, G. Boulon, Structural investigations of Lu_2O_3 as single crystal and polycrystalline transparent ceramic, Cryst. Growth Des. 14 (2014) 3327-3334.
26. R. D. Shannon, Revised effective ionic radii and systematic studies of interatomic distances in halides and chalcogenides, Acta Cryst. A 32 (1976) 751-767.
27. N. D. Todorov, M. V. Abrashev, V. Marinova, M. Kadiyski, L. Dimowa, E. Faulques, Raman spectroscopy and lattice dynamical calculations of Sc_2O_3 single crystals, Phys. Rev. B 87 (2013) 104301.
28. J. Tauc, R. Grigorovici, A. Vancu, Optical properties and electronic structure of amorphous germanium, Phys. Status Solidi B 15 (1966) 627-637.
29. X. Zhang, H. Zhao, S. Gao, Q. Zeng, First-principles study of electronic structure and optical properties of Er:Lu_2O_3, J. Rare Earths (2020), doi: 10.1016/j.jre.2020.03.001.
30. D. E. Zelmon, J. M. Northridge, N. D. Haynes, D. Perlov, K. Petermann, Temperature-dependent Sellmeier equations for rare-earth sesquioxides, Appl. Opt. 52 (2013) 3824-3828 (2013).
31. V. Petrov, K. Petermann, U. Griebner, V. Peters, J. Liu, M. Rico, P. Klopp, G. Huber, Continuous-wave and mode-locked lasers based on cubic sesquioxide crystalline hosts, Proc. SPIE 6216 (2006) 62160H.
32. B. Aull, H. Jenssen, Vibronic interactions in Nd:YAG resulting in nonreciprocity of absorption and stimulated emission cross sections, IEEE J. Quantum Electron. 18 (1982) 925-930.
33. S. A. Payne, L. L. Chase, L. K. Smith, W. L. Kway, W. F. Krupke, Infrared cross-section measurements for crystals doped with Er^{3+}, Tm^{3+} and Ho^{3+}, IEEE J. Quantum Electron. 28 (1992) 2619-2630.
34. K. Petermann, G. Huber, L. Fornasiero, S. Kuch, E. Mix, V. Peters, S. A. Basun, Rare-earth-doped sesquioxides, J. Lumin. 87 (2000) 973-975.
35. Y. Guyot, M. Guzik, G. Alombert-Goget, J. Pejchal, A. Yoshikawa, A. Ito, T. Goto, G. Boulon, Assignment of Yb^{3+} energy levels in the C_2 and C_{3i} centers of Lu_2O_3 sesquioxide either as ceramics or as crystal, J. Lumin. 170 (2016) 513-519.

36. J. M. Serres, V. Jambunathan, P. Loiko, X. Mateos, H. Yu, H. Zhang, J. Liu, A. Lucianetti, T. Mocek, K. Yumashev, U. Griebner, V. Petrov, M. Aguiló, F. Díaz, Microchip laser operation of Yb-doped gallium garnets, Opt. Mater. Express 6 (2016) 46-57.

List of figure captions

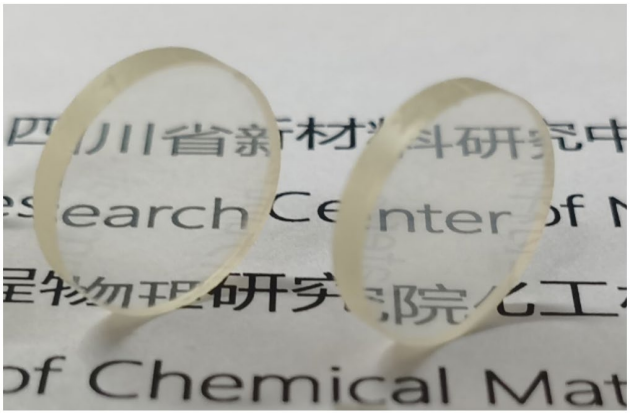

Fig. 1. Photograph of annealed and polished 10 at.% Yb:$(Lu,Sc)_2O_3$ ceramic disks.

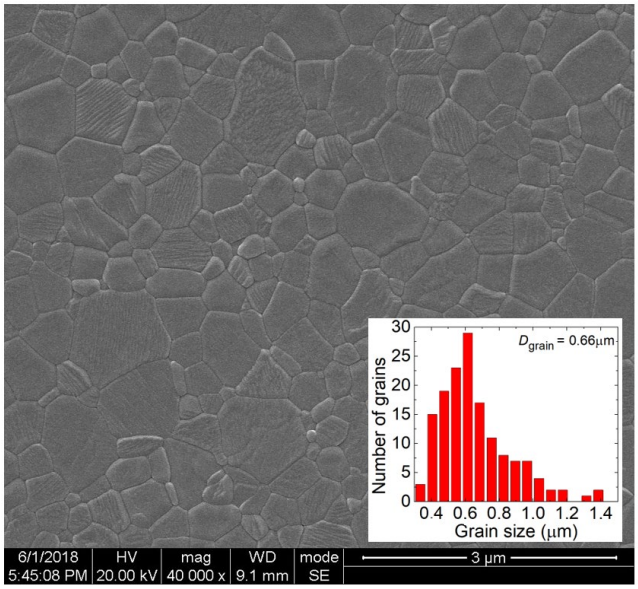

Fig. 2. Field-emission SEM image of the thermally etched surface of the Yb:$(Lu,Sc)_2O_3$ ceramic disk, *inset* – grain size distribution.

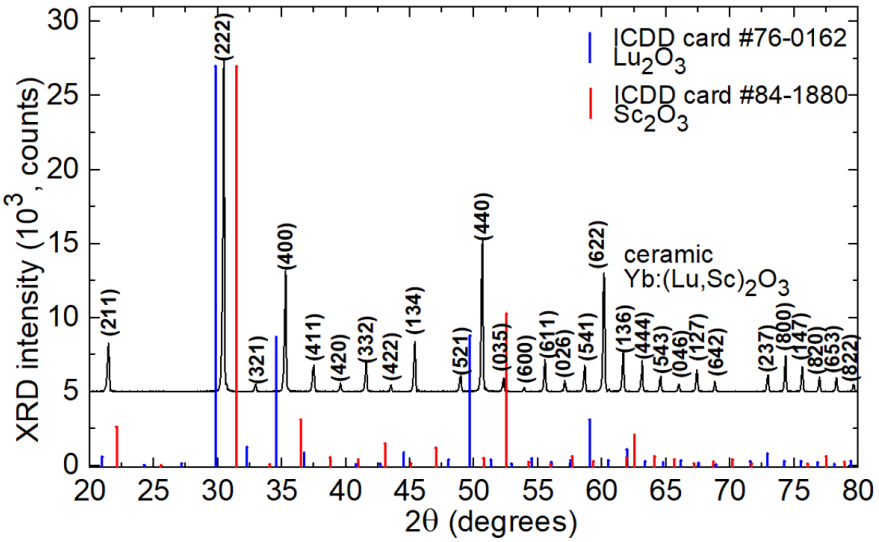

Fig. 3. X-ray powder diffraction pattern of 10 at.% Yb:$(Lu,Sc)_2O_3$ ceramics, *red and blue peaks* – theoretical patterns for Lu_2O_3 (ICDD card #76-0162) and Sc_2O_3 (ICDD card #84-1880), *numbers* – Miller's indices (*hkl*).

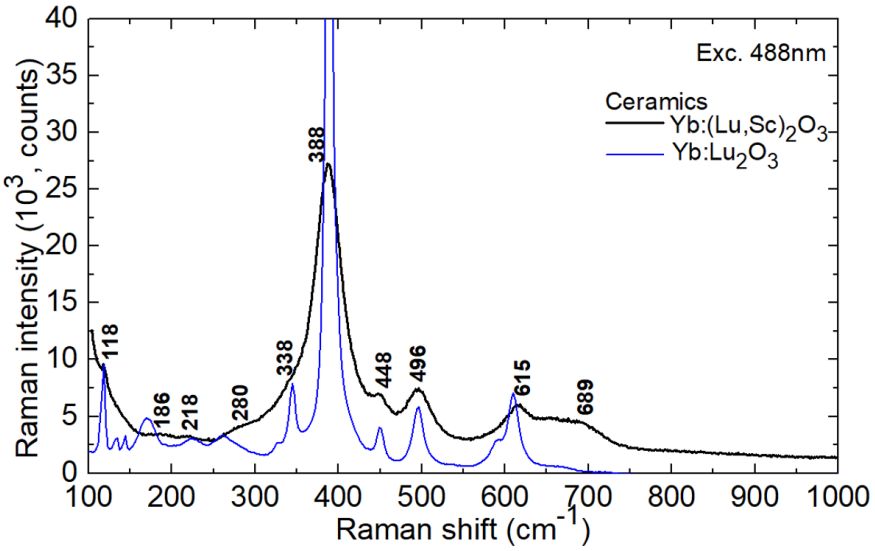

Fig. 4. RT Raman spectrum of Yb:$(Lu,Sc)_2O_3$ ceramics. The spectrum for Yb:Lu_2O_3 is shown for comparison, *numbers* – peak Raman frequencies, λ_{exc} = 488 nm.

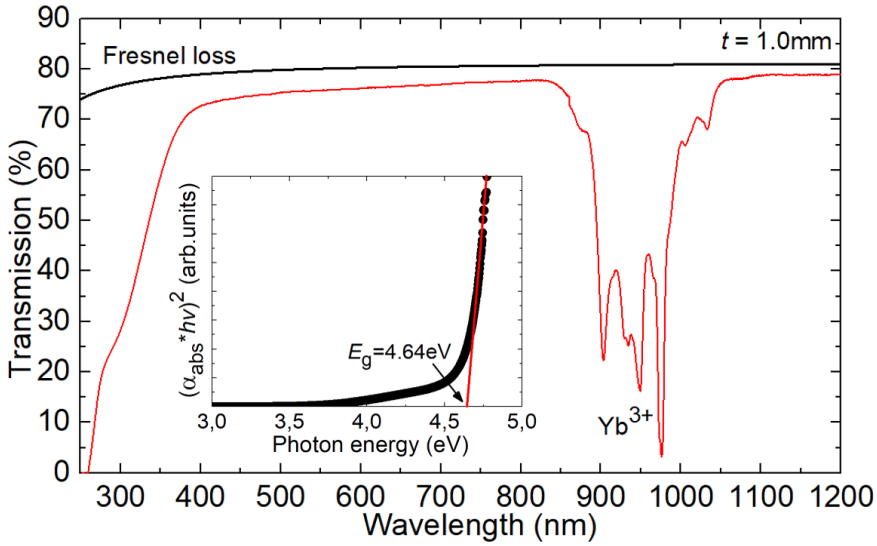

Fig. 5. Transmission spectrum of a laser-grade-polished Yb:$(Lu,Sc)_2O_3$ ceramic disk (thickness, t = 1.0 mm), *black curve* – theoretical transmission determined by the Fresnel losses for $(Lu_{2/3}Sc_{1/3})_2O_3$. *Inset* – Tauc plot for determination of the optical bandgap E_g (assuming direct transitions).

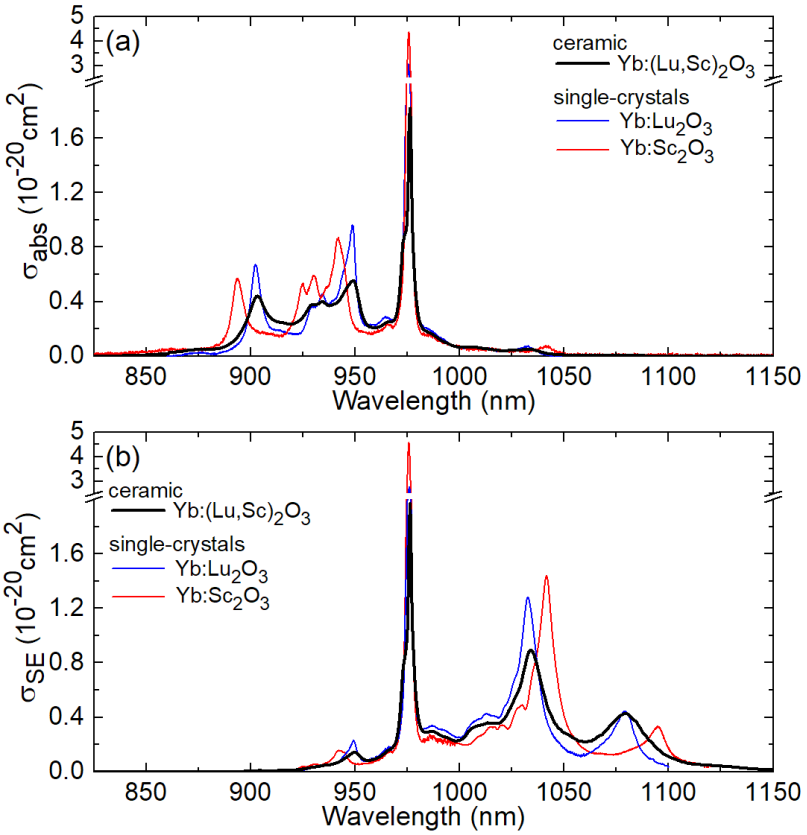

Fig. 6. (a) Absorption cross-sections, σ_{abs}, and (b) stimulated-emission cross-sections, σ_{SE}, for the $^2F_{7/2} \leftrightarrow {}^2F_{5/2}$ Yb^{3+} transition in $(Lu,Sc)_2O_3$ ceramics at RT. The spectra for bulk Yb:Lu_2O_3 and Yb:Sc_2O_3 crystals are given for comparison.

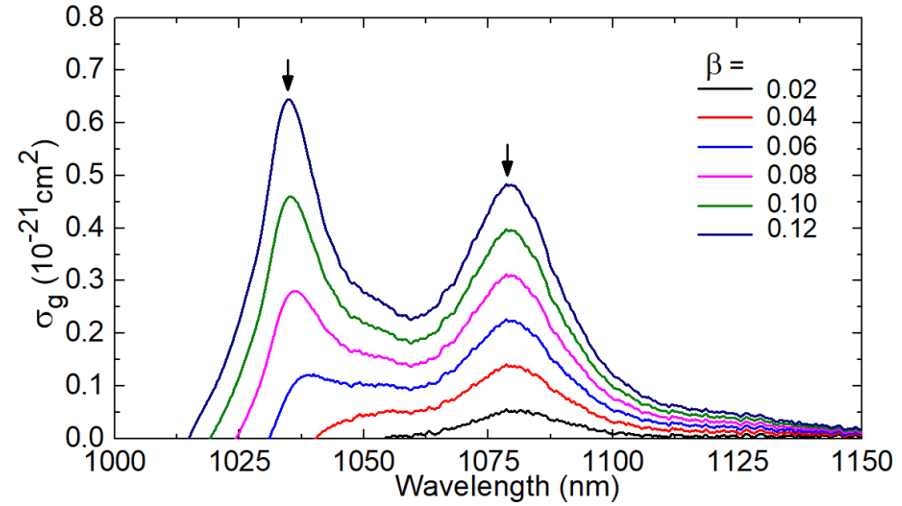

Fig. 7. RT gain cross-sections, $\sigma_g = \beta\sigma_{SE} - (1 - \beta)\sigma_{abs}$, for the $^2F_{7/2} \leftrightarrow {}^2F_{5/2}$ Yb^{3+} transition in $(Lu,Sc)_2O_3$ ceramics for different inversion ratios $\beta = N_2(^2F_{5/2})/N_{Yb}$, *arrows* indicate the observed laser wavelengths.

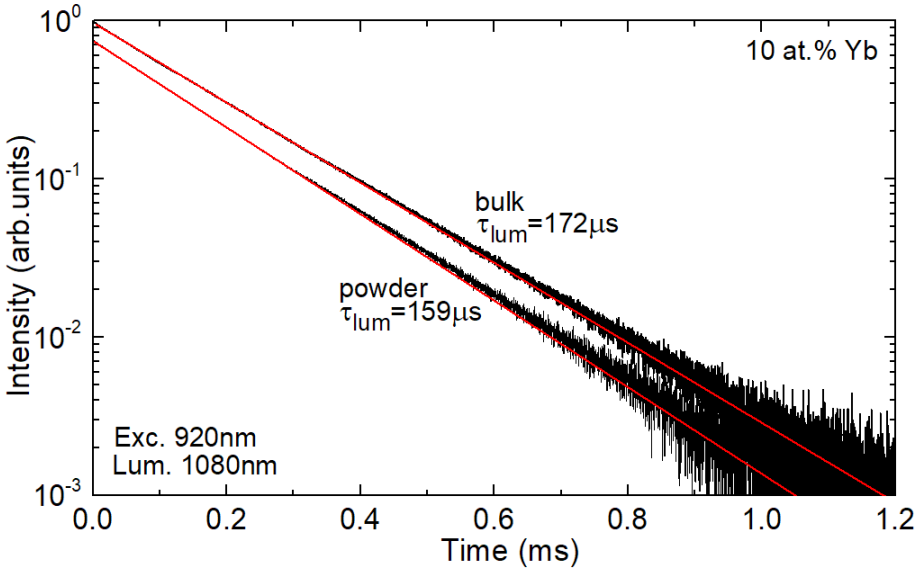

Fig. 8. RT luminescence decay curve for the 10 at.% Yb:$(Lu,Sc)_2O_3$ ceramics (bulk and powdered samples), λ_{exc} = 920 nm, λ_{lum} = 1080 nm, *lines* – single-exponential fits.

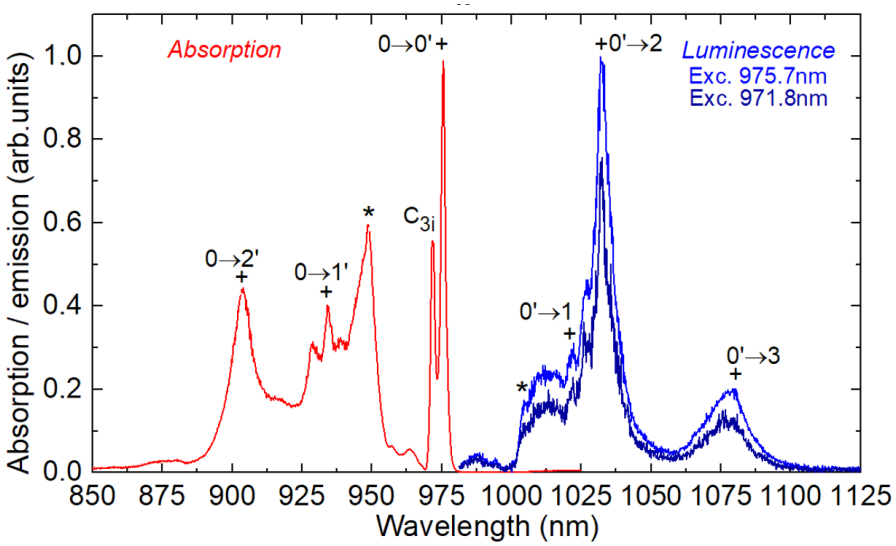

Fig. 9. LT (12 K) absorption and luminescence spectra for the Yb:$(Lu,Sc)_2O_3$ ceramics, λ_{exc} = 975.7 and 971.8 nm, the symbol "+" refers to electronic transitions of Yb^{3+} ions in C_2 sites, *asterisks* refer to the assignment from Ref. [35].

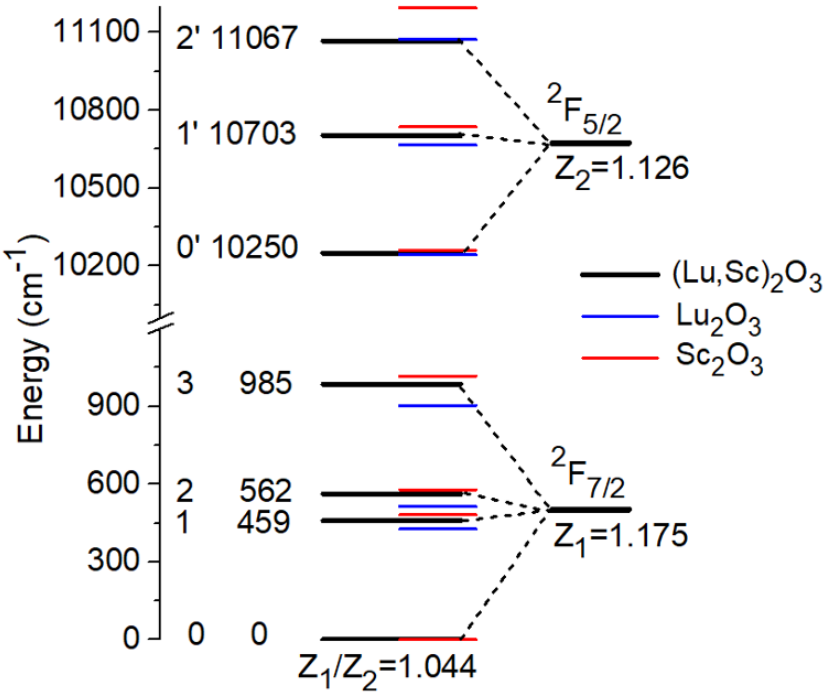

Fig. 10. Crystal-field splitting of Yb^{3+} ions in C_2 sites in the $(Lu,Sc)_2O_3$ ceramics, Stark splitting for Lu_2O_3 and Sc_2O_3 are given for comparison.

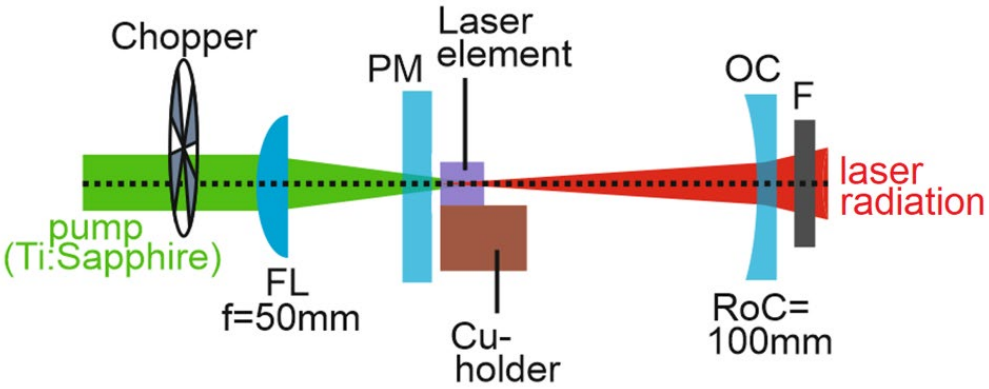

Fig. 11. Scheme of the laser set-up: FL – focusing lens, PM – pump mirror, OC – output coupler, F – cut-on filter.

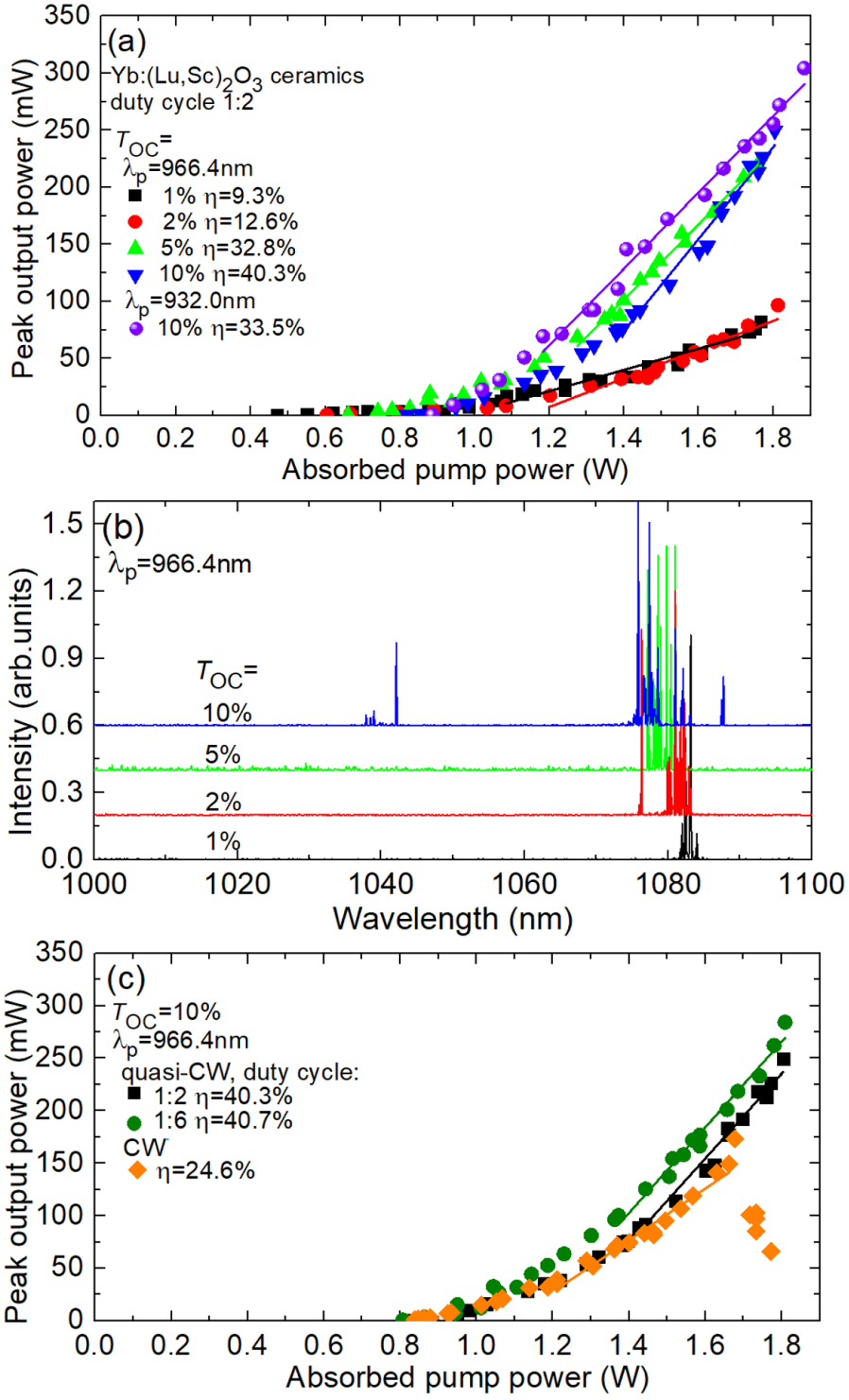

Fig. 12. 10 at.% Yb:$(Lu,Sc)_2O_3$ ceramic laser: (a) input-output dependences, η – slope efficiency, (b) typical spectra of laser emission captured at P_{abs} ~1.6 W, λ_P = 966.4 nm. Quasi-CW pumping, duty cycle: 1:2; (c) Comparison of CW and quasi-CW laser performance for T_{OC} = 10%, λ_P = 966.4 nm.

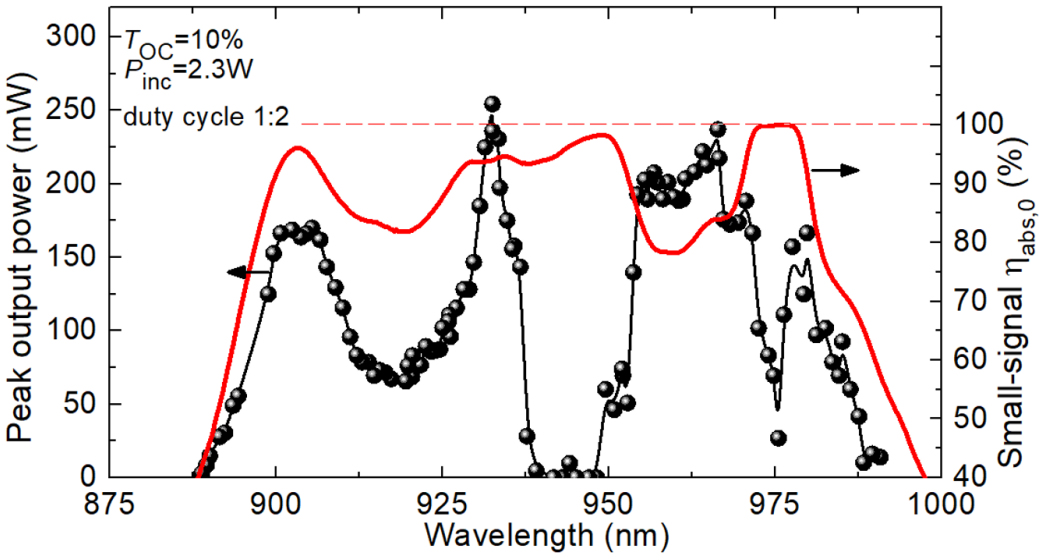

Fig. 13. Laser excitation spectrum for the Yb:$(Lu,Sc)_2O_3$ ceramic laser: peak output power vs. the pump wavelength, T_{OC} = 10%, P_{inc} = 2.1 W, duty cycle: 1:2. The small-signal single-pass pump absorption is given for comparison.